

# POP: Prior-fitted Optimizer Policies

Jan Kobiolka<sup>1</sup> Christian Frey<sup>1</sup> Gresa Shala<sup>2</sup> Arlind Kadra<sup>1</sup> Erind Bedalli<sup>3</sup> Josif Grabocka<sup>1</sup>

## Abstract

Optimization refers to the task of finding extrema of an objective function. Classical gradient-based optimizers are highly sensitive to hyperparameter choices. In highly non-convex settings their performance relies on carefully tuned learning rates, momentum, and gradient accumulation. To address these limitations, we introduce POP (Prior-fitted Optimizer Policies), a meta-learned optimizer that predicts coordinate-wise step sizes conditioned on the contextual information provided in the optimization trajectory. Our model is learned on millions of synthetic optimization problems sampled from a novel prior spanning both convex and non-convex objectives. We evaluate POP on an established benchmark including 47 optimization functions of various complexity, where it consistently outperforms first-order gradient-based methods, non-convex optimization approaches (e.g., evolutionary strategies), Bayesian optimization, and a recent meta-learned competitor under matched budget constraints. Our evaluation demonstrates strong generalization capabilities without task-specific tuning.

## 1. Introduction

Optimization lies at the core of modern machine learning, scientific computing, and engineering. In practice, most continuous optimization problems are solved using gradient and momentum-based methods, which scale efficiently to high-dimensional settings (Robbins & Monro, 1951; Kingma & Ba, 2015; Daoud et al., 2022; Liu et al., 2020). Despite their success, the performance of these optimizers is highly sensitive to hyperparameter choices, in particular the learning-rate schedule and momentum coefficients (Tian et al., 2023; Keskar & Socher, 2017; Hassan et al., 2022). Selecting

suitable hyperparameters often requires extensive hyperparameter optimization, which is costly, time-consuming, and difficult to transfer across tasks and domains (Mary et al., 2025; Liao et al., 2022; Schlotthauer et al., 2025).

More recently, learned optimizers have gained increasing interest in the community (Tang & Yao, 2024; Yang et al., 2023; Metz et al., 2022; Cao et al., 2019; Gomes et al., 2021; Vishnu et al., 2020; Ma et al., 2024; Goldie et al., 2024; Lan et al., 2023). In contrast to classical optimization techniques, learned optimizers are typically composed of black-box function approximators (Metz et al., 2020; Vishnu et al., 2020), or they build on hand-designed update rules whose hyperparameters are learned (Kristiansen et al., 2024; Moudgil et al., 2025). Despite promising results, an open challenge remains how to learn an optimizer’s behavior that (i) reduces the need for extensive tuning across tasks and (ii) maintains effective exploration of the objective landscape under constrained budgets, rather than becoming strongly local once the learning rate is annealed over time.

We introduce POP, a meta-learned optimizer trained as a continuous-control agent leveraging RL meta-learning with optimization specific reward shaping. POP learns a policy that outputs coordinate-wise step size decisions conditioned on the optimization history accumulated over time, which enables our model to be adaptive towards exploration-exploitation trade-offs automatically. Our model leverages a transformer-based backbone (Vaswani et al., 2017) to encode historical long-range trajectory context. Inspired by prior-data fitted networks (PFNs) (Müller et al., 2022), we meta-train our model on a distribution of objective functions drawn from a novel prior. We construct this prior using a Gaussian process (Rasmussen & Williams, 2006), approximated via Random Fourier Features (Rahimi & Recht, 2007), that allows scalable training on a set of diverse objective landscapes at low computational cost.

We illustrate the benefit of a state-conditioned optimizer in Figure 1. POP increases the learning rate when the optimization landscape is sufficiently smooth, enabling rapid convergence to a local minimum. Upon reaching such a minimum, POP can either refine the solution through smaller updates or promote exploration by leveraging information from other regions of the landscape. This adaptive behavior emerges from the policy that is meta-learned to escape local

<sup>1</sup>Department of Computer Science and Artificial Intelligence, University of Technology Nuremberg, Germany <sup>2</sup>Department of Computer Science, Albert Ludwig University of Freiburg, Germany <sup>3</sup>Faculty of Natural Sciences, University of Elbasan, Albania. Correspondence to: Jan Kobiolka <jan.kobiolka@utn.de>.

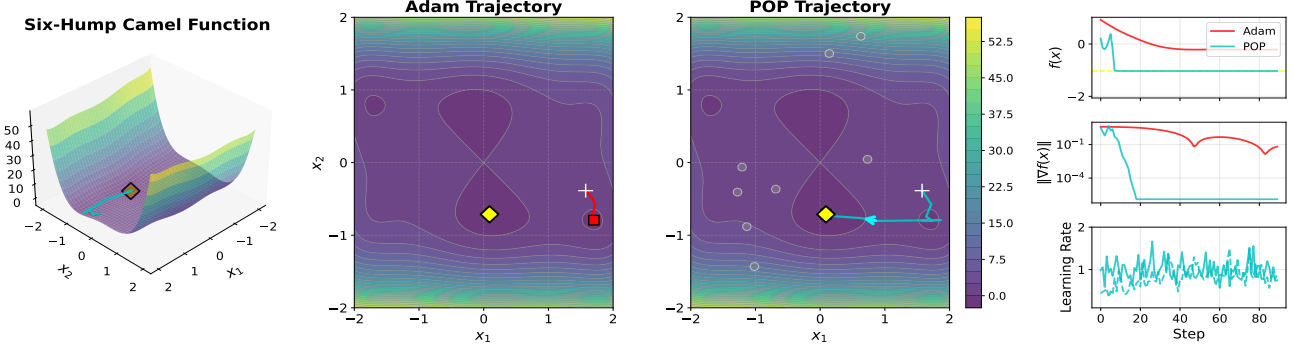


Figure 1. POP (blue) adapts its learning rate based on the optimization landscape, enabling rapid convergence, escape from local minima, and improved global optimization compared to Adam (red). Yellow diamond represents the global minima, the white cross represents the start state, and the square represents the end state.

optima over a plethora of pretraining functions.

A thorough evaluation highlights POP’s generalization on the *Virtual Library of Simulation Experiments* (Surjanovic & Bingham) benchmark consisting of 47 diverse optimization functions. We further evaluate our model’s capabilities to transfer to longer optimization horizons and higher-dimensional problems. A statistical ranking analysis reveals that our method outperforms classical optimizers as well as a meta-learned optimizer introduced recently under matched budget constraints. The key contributions of this paper are:

- We introduce POP, a novel optimizer that is meta-trained over millions of functions and learns step size policies conditioned on the optimization’s contextual information, enabling effective exploration-exploitation behavior during optimization.
- A Gaussian process-based prior that combines convex and non-convex objectives, enabling scalable meta-training on diverse optimization landscapes and supporting strong generalization.
- An empirical evaluation on 47 benchmark functions showing superior performance over conventional optimizers, with ablations on reward design, evaluation budget, and scalability to higher dimensions.

## 2. POP: Prior-fitted Optimizer

In the following, we consider unconstrained optimization problems of the form  $x^* \in \operatorname{argmin}_{x \in \mathbb{R}^d} f(x)$ , where each task instance is an objective function  $f$  sampled from a prior  $f \sim p(f)$  over the space of compact functions. We refer to an episode as optimizing a single sampled function  $f$  for a fixed budget of  $T$  time steps. We define an optimization trajectory as:

**Definition 2.1** (Optimization trajectory). For an objective function  $f$ , we define the optimization trajectory that in-

cludes the first  $t$  update steps of a maximum budget of  $T$  updates as:

$$\tau^{(t)} := \left\{ \left( x_i, y_i, \nabla f(x_i), \frac{i}{T} \right) \right\}_{i=1}^t, \quad (1)$$

where  $x_i$  denotes the parameters of the optimization problem in step  $i$ , while  $y_i := f(x_i)$  is the function value,  $\nabla f(x_i)$  the gradient information, and  $\frac{i}{T}$  the normalized timestep.

First-order optimizers proceed by applying an update rule based on local gradient information, e.g., GD applies  $x_t = x_{t-1} - \eta_t \nabla f(x_{t-1})$ , where  $\eta_t$  is the step size at iteration  $t$ . In this work, we replace a preset step size schedule by a meta-learned policy  $\eta_t \sim \pi_\theta(\eta_t | \tau^{(t-1)})$ , where at each iteration, our optimizer outputs the next step size  $\eta_t$  via a state-conditioned control signal  $\tau^{(t-1)}$  based on the optimization trajectory (cf. Theorem 2.1) up to step  $t-1$ .

### 2.1. MDP for Optimization

We formulate the optimization problem as a Markov Decision Process (MDP) defined by the tuple  $(\mathcal{S}, \mathcal{A}, \mathcal{P}, r, p_0, \gamma)$ , where  $\mathcal{S}$  are the states,  $\mathcal{A}$  the actions,  $\mathcal{P}$  the transition dynamics,  $r : \mathcal{A} \times \mathcal{S} \rightarrow \mathbb{R}$  denotes the reward signal,  $p_0$  is the probability distribution of initial elements in the optimization trajectory, and  $\gamma$  denotes the discount factor. Our goal is to train a parameterized policy  $\pi_\theta : \mathcal{S} \times \mathcal{A} \rightarrow \mathbb{R}^+$ .

In our meta-learning setting, an episode corresponds to an optimization trajectory  $\tau$  on a sampled task instance from a prior, i.e.,  $f \sim p(f)$ . In the sequential decision problem, the policy receives a representation of the current optimization context and outputs a continuous coordinate-wise step size action  $a_t = \eta_t \in \mathbb{R}^d > 0$ . The state  $s_t \in \mathcal{S}$  is simply the trajectory of updates so far  $s_t := \tau^{(t)}$ , for  $t \in [1, \dots, T]$ .

### 2.2. Optimization Step

Given an optimization trajectory  $\tau^{(t-1)}$ , our stochastic policy is a network with parameters  $\theta$  that outputs the

update steps at iteration  $t$  for each function dimension  $\mu_\theta(\tau^{(t-1)}) \in \mathbb{R}^d$  and the standard deviation  $\sigma_\theta \in \mathbb{R}^d$ .

$$\pi_\theta(\eta_t | \tau^{(t-1)}) = \mathcal{N}(\mu_\theta(\tau^{(t-1)}), \text{diag}(\sigma_\theta^2)) \quad (2)$$

To conduct an optimization, POP applies three steps. First, it samples a coordinate-wise next step size from our policy network (Equation 3). Then, POP conducts a gradient update (Equation 4), and finally, it updates the trajectory (Equation 5).

$$\eta_t \sim \pi_\theta(\eta_t | \tau^{(t-1)}) \quad (3)$$

$$x_t \leftarrow x_{t-1} - \eta_t \nabla f(x_{t-1}) \quad (4)$$

$$\tau^{(t)} \leftarrow \tau^{(t-1)} \cup \left\{ \left( x_t, y_t, \nabla f(x_t), \frac{t}{T} \right) \right\} \quad (5)$$

### 2.3. Reward Signal

We use a dedicated reward function for our optimization, defined as the improvement to the best observed function value so far in a trajectory. Let  $y_{t-1}^* = \min_{(\cdot, y, \cdot, \cdot) \in \tau^{(t-1)}} y$ , we define:

$$R(y_t, \tau^{(t-1)}) = \max(0, y_{t-1}^* - y_t). \quad (6)$$

This reward assigns a positive signal only when an action yields a new observed minimum, directly linking policy optimization to objective improvement. Since non-improving steps receive no penalty, the agent can explore the function freely, and meaningful improvements guide learning.

### 2.4. Meta-Learning Objective

We optimize the policy parameters  $\theta$  to maximize the expected return over tasks sampled from a prior (cf. Section 3). We formulate the objective as follows:

$$\max_{\theta} \mathbb{E}_{f \sim p(f)} \mathbb{E}_{\tau \sim \text{POP}(f; \theta)} \sum_{t=0}^T \gamma^t R(y_t, \tau^{(t-1)}), \quad (7)$$

where  $\tau \sim \text{POP}(f; \theta)$  is computed by running Equations 3–5 for  $T$  steps on the function  $f$  sampled from the prior. We train the policy parameters using the Proximal Policy Optimization (PPO) algorithm (Schulman et al., 2017).

## 3. A Prior for Optimization Problems

In order to meta-train our method, we sample optimization problems from a prior distribution  $f \sim p(f)$ . This distribution must be sufficiently diverse and complex to cover a wide range of optimization problems, including both convex and non-convex functions, so that learned optimizers generalize well across problems. Therefore, we

define a prior over optimization objectives as a combination of a separable quadratic (convex) component and a Gaussian process prior with an RBF kernel, approximated via *Random Fourier Features* (RFF) for computational efficiency (Rahimi & Recht, 2007). We define a mixing weight  $\alpha \sim \mathcal{U}(\alpha_{\min}, \alpha_{\max})$  that interpolates between the convex and non-convex components. For a given dimensionality  $D$ , functions are constructed as:

$$f(x) := \alpha f_C(x) + (1 - \alpha) f_{\text{RFF}}(x), \quad (8)$$

with the convex component defined as:

$$f_C(x) = \sum_{d=1}^D \beta_d^1 (x_d - \beta_d^2)^2, \quad (9)$$

where  $\beta_d^1 \sim \mathcal{U}(\beta_{\min}^1, \beta_{\max}^1)$  controls the curvature and ensures convexity, and  $\beta_d^2 \sim \mathcal{U}(\beta_{\min}^2, \beta_{\max}^2)$  determines the location of the quadratic minimum. With probability  $p_{\text{convex}}$  we set  $\alpha = 1$ , yielding strictly convex quadratic objectives.

The RFF Gaussian process prior is constructed as:

$$f_{\text{RFF}}(x) = \sqrt{2} \sum_{m=1}^M \omega_m^1 \cos((\omega_m^2)^\top x + \omega_m^3). \quad (10)$$

The Gaussian process approximation uses  $M$  Random Fourier Features with phases  $\omega_m^3 \sim \mathcal{U}(0, 2\pi)$ , weights  $\omega_m^1 \sim \mathcal{N}(0, \sigma^2/M)$ , and frequencies  $\omega_m^2 \sim \mathcal{N}(\mathbf{0}, \ell^{-2} \mathbf{I}_D)$ . The lengthscale  $\ell \sim \mathcal{U}(\ell_{\min}, \ell_{\max})$  controls the smoothness of the resulting functions, while the output scale  $\sigma \sim \mathcal{U}(\sigma_{\min}, \sigma_{\max})$  controls their amplitude. The  $1/M$  scaling of  $\omega_m^1$  ensures that the variance of  $f_{\text{RFF}}$  remains bounded as  $M$  increases.

To sample a new function, we simply sample the new hyperparameters  $\alpha$ ,  $\ell$ , and  $\sigma$ . For the new hyperparameters, we then sample new  $\beta \in \mathbb{R}^{2 \times D}$  and  $\omega \in \mathbb{R}^{3 \times D}$ . In Section A, we prove that drawing functions from a GP-based prior is universal and every possible function in a compact set can be approximately drawn from a GP with random hyperparameters.

## 4. In-Distribution Generalization

One of the major challenges when meta-learning an optimizer’s policy is the mismatch of domains and ranges across functions, leading to out-of-distribution failures (i.e., naively meta-learned policies fail for functions having very similar shapes but different scales). To ensure that our policy will be meta-learned and transferred to matching functions under an in-distribution assumption, we transform the domains and ranges of all training and test functions identically.

**Initial Context.** POP trains deep parametric policies that output the next learning rate based on the trajectory of observations so far, therefore, transferring knowledge from

previously-seen functions with a similar landscape. Therefore, it needs an initial trajectory as an input before it conducts the first update step.

As the initial context for our policy at the beginning of the optimization, we sample  $c \in \mathbb{N}^+$  observations. Let  $p_0 \in \mathcal{P}(x)$  denote a random initial probability measure on the parameter space, where  $\mathcal{P}(x)$  is the set of probability distributions on a functions' parameter space. We define  $s_c \sim p_0 \Leftrightarrow s_c := \tau^{(c)}$ . After sampling the initial random context, we use the  $x_i$  with the lowest  $f(x_i)$  as the starting point of the gradient descent update steps leveraging coordinate-wise step sizes.

**Boundary Scaling.** For each function, we assume known domain coordinate-wise boundaries  $x \in [x^{\min}, x^{\max}]$  and map coordinates to a fixed symmetric interval via boundary scaling per dimension.

$$x_t^{\text{bnd}} = V_x \cdot \left( 2 \cdot \frac{x_t - x^{\min}}{x^{\max} - x^{\min}} - 1 \right) \quad \text{with } V_x \in \mathbb{R}^+. \quad (11)$$

where  $V_x$  refers to the target scale. Analogously, we scale function values using running extrema  $y_{t,\min} := \min_{j \leq t} y_j$  and  $y_{t,\max} := \max_{j \leq t} y_j$ , initialized from the random context  $s_c$  and update them online when the function's landscape is explored and the context information increases:

$$y_t^{\text{bnd}} = V_y \cdot \left( 2 \cdot \frac{y_t - y_t^{\min}}{y_t^{\max} - y_t^{\min}} - 1 \right) \quad \text{with } V_y \in \mathbb{R}^+. \quad (12)$$

where  $V_y$  refers to the target scale.

**Z-transformation.** Boundary-scaled  $x_t^{\text{bnd}}$  and  $y_t^{\text{bnd}}$  are then standardized by applying an online Z-transformation using the evaluation data of the current optimization trajectory, yielding  $\tilde{x}_t$  and  $\tilde{y}_t$ .

**Gradient Scaling.** Because  $\tilde{x}_t, \tilde{y}_t$  are transformed before being passed to the model, gradients defined in the original coordinates are no longer consistent with the transformed space. We therefore apply the corresponding Jacobian to obtain gradients that reflect the correct local sensitivities:

$$\nabla \tilde{f}(x_t) = \left( \frac{\sigma_{x,t}}{\sigma_{y,t}} \right) \left( \frac{V_y}{V_x} \right) \left( \frac{x^{\max} - x^{\min}}{y_t^{\max} - y_t^{\min}} \right) \odot \nabla f(x_t), \quad (13)$$

with  $V_x, V_y \in \mathbb{R}^+$  denoting coordinate-wise scaling parameters, and  $\sigma_{x,t}, \sigma_{y,t}$  denoting the standard deviation of the respective dimension up to time step  $t$ . The optimizer maintains one state per coordinate, defined exclusively in the transformed space.

**Transformed Update.** Since the model operates on the transformed variables  $\tilde{\tau}^{(t-1)}$ , the gradient update is performed in the transformed space. Specifically,  $\tilde{x}_t = \tilde{x}_{t-1} - \eta_t \nabla \tilde{f}(x_{t-1})$ . The updated iterate  $\tilde{x}_t$  is then mapped back to the original domain by applying the inverse Z-transformation followed by inverse boundary scaling, after

which it is evaluated using the original objective function  $f(x_t)$ . Following the evaluation of the new  $x_t$ ,  $y_t$ , and  $\nabla f(x_t)$ , the entire transformed set  $\tilde{\tau}^{(t)}$  is re-transformed using the updated statistics.

## 5. Experimental Protocol

We train our proposed optimizer (cf. Section 2) on our newly proposed prior (cf. Section 3), with parameter distributions detailed in Table 4 in Appendix B.1. Notably, we restrict our prior to two-dimensional ( $D=2$ ) objective functions. Visualizations of randomly sampled functions from this prior are shown in Section B.2. Rather than conditioning on the full optimization trajectory  $\tau^{(t-1)}$ , we decompose trajectories along dimensions and restrict the policy input to the history of the corresponding coordinate. The optimizer thus operates independently per dimension, enforcing conditional independence during training while enabling efficient batching and scalability to higher-dimensional problems. We open-source our implementation<sup>1</sup> to foster future research.

### 5.1. Architecture and Training

We parameterize both the actor and critic using a shared transformer backbone with separate MLP heads, for a total of  $166K$  trainable parameters. Full architectural and training hyperparameters are reported in Tables 5 and 6. The actor outputs the mean of a Gaussian policy and samples actions using a learned, state-independent log standard deviation. For numerical stability, the log standard deviation is passed through a tanh nonlinearity and rescaled to lie in  $[-3.0, 2.0]$ . To enforce strictly positive learning rates, sampled actions are exponentiated via  $\exp(\eta_t)$ .

We sample  $B = 256$  optimization problems per training iteration and train for 50,000 iterations, yielding approximately  $1.28 \times 10^7$  optimization problem instances. The objective function is resampled from the prior every 8 iterations, resulting in  $1.6 \times 10^6$  distinct functions. At the beginning of each iteration, a random initial context of  $c = 10$  points is generated, after which the agent is rolled out for  $T = 40$  optimization steps to solve a single optimization problem and collect trajectories. Following each rollout, the policy and value networks are updated using PPO on the collected transitions. Training requires approximately 10 hours on a single NVIDIA H100 GPU.

### 5.2. Benchmarks

**In-distribution Performance.** We construct a validation set for ablations consisting of 1024 optimization problems in  $D=2$ , and test sets for one-shot evaluation with 1024 problems each for  $D \in \{2, 8, 16, 32\}$ . All problems use a

<sup>1</sup><https://anonymous.4open.science/r/pop-F342/README.md>

fixed initial context of size  $c=10$ .

**Out-of-distribution Experiments.** We further evaluate the out-of-distribution performance of our method on 47 optimization problems from the widely used Virtual Library of Simulation Experiments (VLSE) benchmark (Surjanovic & Bingham). It covers a diverse range of optimization landscapes, including functions with many local minima, as well as bowl-shaped, plate-shaped, and valley-shaped geometries, in addition to steep ridges and drops. Each benchmark problem is evaluated at its native dimensionality, which ranges from 1D to 6D across the suite.

### 5.3. Baselines

We compare our method against a diverse set of optimization baselines. **Gradient Descent (GD)** (Cauchy, 1847) and **Adam** (Kingma & Ba, 2015) represent first-order gradient-based methods, with Adam using adaptive learning rates. **L-BFGS** (Liu & Nocedal, 1989) is a quasi-Newton method leveraging approximate second-order information. **Random Search** provides a simple derivative-free baseline, while **Genetic Algorithms** (Holland, 1992) and **Differential Evolution** (Storn & Price, 1997) are population-based evolutionary methods for global optimization. **TPE** (Bergstra et al., 2011) is a Bayesian optimization approach that models the objective to guide sample selection. Lastly, **VeLo** (Metz et al., 2022) is a learned optimizer which has been trained on a prior of neural network architectures. All baselines are evaluated under the same optimization budget.

## 6. Evaluation

### Hypothesis 1: Learned optimizers trained on synthetic priors can generalize to unseen problems from the same distribution.

Initially, we evaluate if POP can generalize to unseen problems drawn from the same distribution. Performance is measured using normalized improvement, which captures how much the optimizer improves beyond the best value observed in the initial context, while normalizing by the context’s objective range to ensure comparability across problems:

$$NI = \frac{y_t^{\min} - y_t^*}{y_t^{\max} - y_t^{\min} + \epsilon} \quad (14)$$

where  $y_{t,\min} := \min_{j \leq t} y_j$  denotes the smallest loss value in the initial context and  $y_t^* = \min_{(\cdot, y, \cdot, \cdot) \in \tau^{(t-1)}} y$  is the best loss value achieved in the optimization trajectory so far. We include a small  $\epsilon$  for numerical stability when the context range is close to zero. In Figure 2, we provide the episode rewards and the normalized improvement on the validation set during training. As observed, the normalized improvement increases together with the training reward,

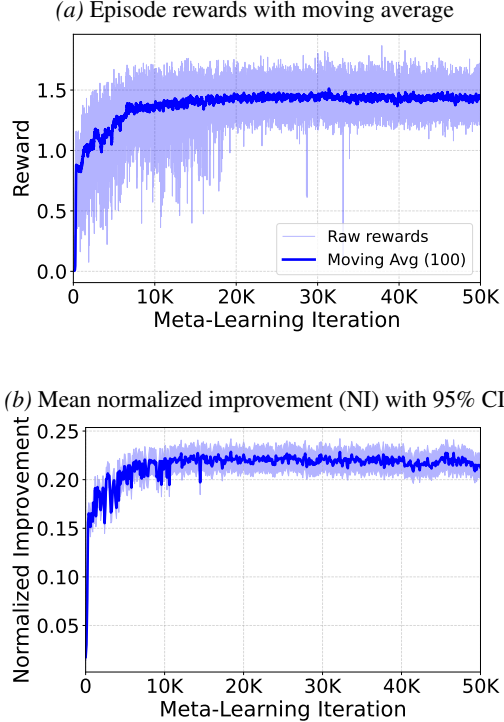


Figure 2. Meta-learning reward and evaluation validation performance of our POP agent.

indicating successful within-distribution generalization on unseen problems. We further find that POP is capable of inferring the shape of the objective function from context and adjusting its behavior accordingly. For convex functions, POP rapidly converges to a local minimum and subsequently refrains from further exploration of the function landscape. In contrast, for non-convex functions, POP explores local minima, strategically escapes them, and repeatedly converges to new local minima. A visual illustration of this behavior is provided in Section D.1.

Next, we evaluate the competitiveness of our method by comparing it against a set of baselines such as GD, Adam, L-BFGS, and Random search on unseen test problems drawn from the same prior distribution. Since we require  $c$  initial context points, we initialize all methods with identical context sets. For gradient-based methods, we select the best-performing context point as the initialization. We additionally tune the learning rate for GD, Adam and L-BFGS using grid search on the validation set (hyperparameter settings are detailed in Section C) and leave the other parameter values at their default setting. We evaluate all methods on the test set.

As shown in Figures 3 and 4, POP outperforms all baselines by achieving higher normalized improvement during optimization, while gradient-based baselines plateau earlier, and random search improves more slowly. The initial strong

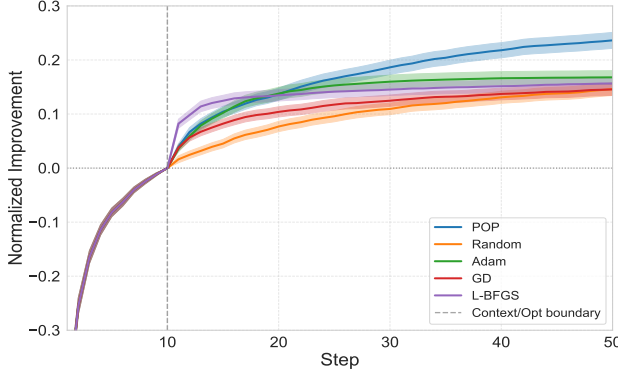


Figure 3. In-distribution test set performance vs. baselines. Mean normalized improvement over steps; shading indicates 95% CIs. Dashed line marks the context/optimization boundary.

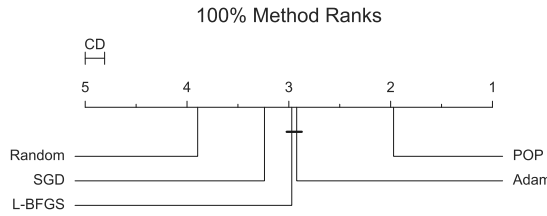


Figure 4. Method rankings on the in-distribution test set at 100% budget. Lower ranks correspond to better performance, while horizontal bars indicate differences that are not statistically significant.

performance of L-BFGS can be attributed to its substantially higher number of function evaluations per iteration compared to the other methods, which provides an early advantage but leads to earlier plateauing.

We next conduct a series of ablation studies to evaluate our design choices, focusing on the reward formulation and action parameterization.

**Reward Formulation.** We compare five reward functions that differ in how they incentivize improvement. Let  $\tilde{y}_t$  denote the boundary scaled and Z-transformed current objective value and  $\tilde{y}_{t-1}^*$  the boundary scaled and Z-transformed best value observed in the optimization trajectory. The corresponding reward functions are defined as :

$$R_{\text{Current}} = \tilde{y}_t, \quad (15)$$

$$R_{\text{Global Imp}} = \tilde{y}_{t-1}^* - \tilde{y}_t, \quad (16)$$

$$R_{\text{Global Imp}_c} = \max(0, \tilde{y}_{t-1}^* - \tilde{y}_t), \quad (17)$$

$$R_{\text{SMAPE}} = \max\left(0, \frac{2 \cdot \max(0, \tilde{y}_{t-1}^* - \tilde{y}_t)}{|\tilde{y}_{t-1}^*| + |\tilde{y}_t|}\right), \quad (18)$$

$$R_{\text{Mix},\alpha} = \alpha \max(0, \tilde{y}_{t-1}^* - \tilde{y}_t) + (1 - \alpha) (\tilde{y}_{t-1} - \tilde{y}_t). \quad (19)$$

We evaluate each on the within-distribution validation set with identical starting context. Table 1 shows that  $R_{\text{Global Imp}_c}$  achieves the highest mean normalized improve-

Table 1. Reward ablation on in-distribution validation set. Mean normalized improvement (higher is better) after 50k training iterations with 95% CIs.

Method	Mean	CI <sub>95%</sub> low	CI <sub>95%</sub> high
$R_{\text{Current}}$	0.1917	0.1797	0.2037
$R_{\text{Global Imp}}$	0.1270	0.1179	0.1360
$R_{\text{Global Imp}_c}$	<b>0.2127</b>	0.1998	0.2255
$R_{\text{SMAPE}}$	0.1193	0.1112	0.1274
$R_{\text{Mix},\alpha=0.1}$	0.1454	0.1347	0.1562
$R_{\text{Mix},\alpha=0.2}$	0.1969	0.1846	0.2093
$R_{\text{Mix},\alpha=0.3}$	0.1817	0.1698	0.1935

ment. We attribute this to the fact that clipped rewards do not penalize exploratory actions, allowing the agent to temporarily move away from the current best solution without incurring negative reward, enabling to find better solutions.

#### Action parameterization.

We ablate the choice of action representation used by the policy. In particular, we compare two alternatives: (i) predicting a per-coordinate scalar learning rate and applying a gradient descent update in the transformed state space, and (ii) directly predicting the next iterate  $\tilde{x}_{t+1}$  on a per-coordinate basis in the transformed state space. All other components of the model and training procedure are kept fixed. Table 2 reports the mean performance of both variants, where, predicting the learning rate yields a higher mean, indicating that parameterizing the action as a learning rate is more effective.

Table 2. Action ablation.

Action Mode	Mean
LR	<b>0.2127</b>
Next $x$	0.1986

**Hypothesis 2: Learned coordinate optimizers trained on a low-dimensional (2D) prior for a fixed number of iterations generalizes to longer optimization horizons and higher-dimensional problems.**

To test whether the POP optimizer trained on 2D trajectories generalizes beyond its training regime, we first evaluate performance under a longer optimization budget on unseen test functions sampled from the same prior distribution. Since, we utilize last-token pooling in our architecture, the model is not constrained to the sequence length seen during training. Therefore, we extend the evaluation budget from 50 to 100 iterations, setting  $c=10$  and allowing the model to predict the subsequent  $T=90$  updates. As shown in Figure 5, POP continues to reduce the loss beyond the training horizon and outperforms all baselines over the extended budget.

Next, we evaluate whether POP generalizes to higher-dimensional test problems compared to the 2D problems encountered during training. Due to its coordinate-wise formulation, the optimizer can be applied to higher dimensions by batching across coordinates without architectural modification. We evaluate the model on 8D, 16D, and 32D

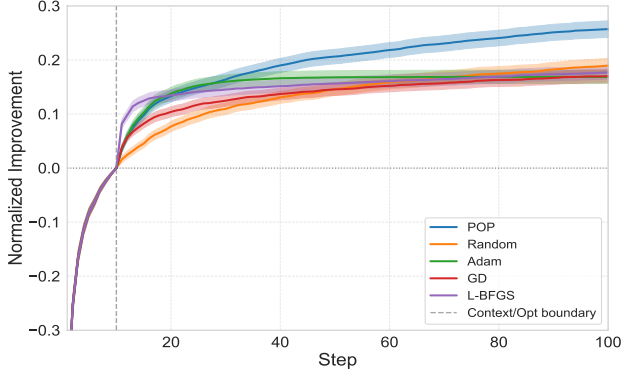


Figure 5. In-distribution test set performance vs. baselines at twice the training budget. Mean normalized improvement over steps; shading indicates 95% CIs. Dashed line marks the context/optimization boundary.

test problems, running each method for 100 optimization steps<sup>2</sup>. For the baselines we zero-shot apply the best found LR’s for the 2D validation set. As shown in Table 3, POP maintains strong performance relative to the baselines even as dimensionality increases.

Table 3. Mean performance across different dimensionalities.

Method	8D	16D	32D
POP	<b>0.2433</b>	<b>0.2467</b>	<b>0.2508</b>
Random	0.1788	0.1789	0.1809
Adam	0.1588	0.1553	0.1622
GD	0.1655	0.1634	0.1642
L-BFGS	0.1833	0.1829	0.1776

### Hypothesis 3: Learned coordinate optimizers trained on a low-dimensional (2D) synthetic prior can generalize to out-of-distribution problems.

We further validate the generalization capabilities of our method on the *Virtual Library of Simulation Experiments* benchmark. Since the optimal hyperparameters for each algorithm on the benchmark are unknown, all baseline methods are evaluated using their default settings. Initially, we compare all methods in terms of per-task normalized regret:

$$r_{\text{opt},t} = \frac{y_t^* - y^{\min}}{y^{\max} - y^{\min}}, \quad (20)$$

where  $y_t^*$  represents the best function value achieved by an optimizer at iteration  $t$  for a given function, while  $y^{\min}$  ( $y^{\max}$ ) represent the minimal (maximal) value of that function.

In Figure 6, we present the average normalized regret for all methods across the different optimization tasks, where POP manages to outperform the majority of methods, and is second only to TPE after 100 optimization trials. For detailed per-function results, we point the reader to Appendix E.

<sup>2</sup>To maintain comparable smoothness across dimensions, the number of parameters is increased to  $M \in \{8000, 16000, 32000\}$ .

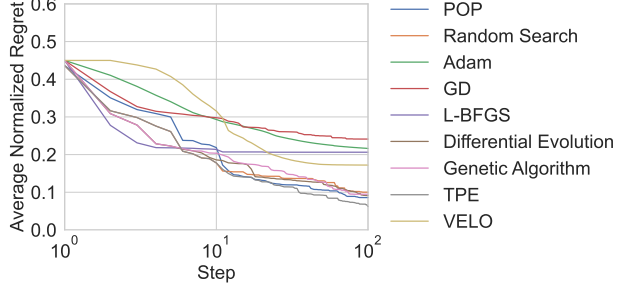


Figure 6. The average normalized regret for all methods. Solid lines represent the mean value.

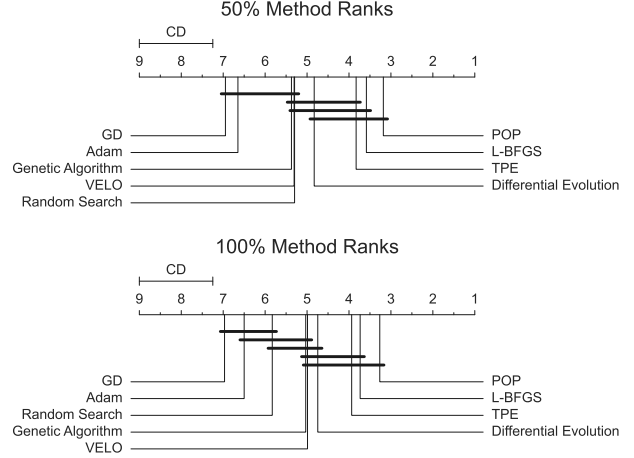


Figure 7. The critical difference diagram, where horizontal bars indicate a lack of statistical significance. A lower rank depicts a better performance. **Top:** Results after 50% of the optimization process has elapsed, **Bottom:** Results at the end of the optimization process.

In Figure 7 we provide critical difference (CD) diagrams, to investigate the method ranks and the statistical significance of the results. To build the CD diagrams, we use the autorank (Herbold, 2020) package that runs a Friedman test with a Nemenyi post-hoc test, at a 0.05 significance level.

The results indicate that POP wins in the majority of tasks and achieves the best rank across all methods. During half of the optimization process (Figure 7 top), POP not only outperforms all baselines, but the difference in results with SGD, Adam, genetic algorithms, VELO, and random search is statistically significant. After the full optimization process has finished (Figure 7 bottom), POP still manages to outperform all baselines in an out-of-distribution scenario, with a significant difference in results to SGD, Adam, and random search.

Lastly, in Figure 8, we investigate the average rank obtained by every method during the optimization procedure, where, after the first 10 random observations for POP, it manages to not only achieve the best final performance, but it has better any-time performance compared to other baselines.

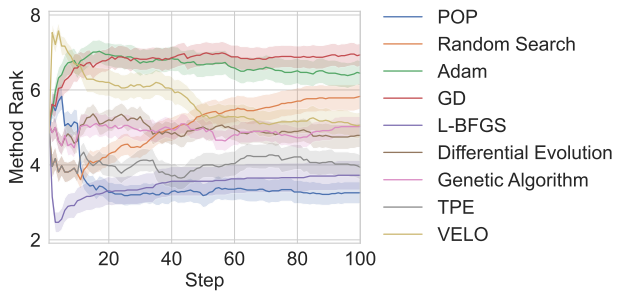


Figure 8. Method ranks during the optimization procedure. The solid lines represent the average rank, while the shaded region represents the standard error.

## 7. Related Work

**Optimizers.** Optimization aims to find the minimum/maximum of a given objective function. Depending on the underlying structure of the function, different optimization methods may be more or less effective. For convex functions, second-order methods such as Newton’s method (Newton, 1736) or quasi-Newton approaches like L-BFGS (Liu & Nocedal, 1989) can be highly efficient. In contrast, for non-convex problems, population-based methods such as *Genetic Algorithms* (Holland, 1992) and *Differential Evolution* (Storn & Price, 1997) are often effective at escaping local minima. For low-dimensional problems, *Bayesian Optimization* (Bergstra et al., 2011) can be particularly powerful, although it scales poorly with increasing dimensionality. In higher-dimensional settings, such as training neural networks, first-order methods including *Gradient Descent* (Cauchy, 1847) and adaptive variants like *Adam* (Kingma & Ba, 2015) are widely used.

**Learned Optimizers.** A growing field that tries to automate the design and tuning of optimization algorithms is known as *Learning to Optimize* (L2O) (Chen et al., 2021; Tang & Yao, 2024). Most L2O approaches meta-train optimizers on neural network training tasks (Metz et al., 2022; Xu et al., 2019; Shu et al., 2020). These methods differ in what aspects of the optimization process are learned, ranging from direct parameter updates (Metz et al., 2022) to the prediction of a global learning rate schedule (Xu et al., 2019; Shu et al., 2020). They also vary in their meta-learning methodology, with some approaches relying on reinforcement learning (Xu et al., 2019), while others employ gradient-based meta-training (Metz et al., 2022; Gärtner et al., 2023).

**Prior-fitted Models.** Prior-Data Fitted Networks (PFN) (Müller et al., 2022; Hollmann et al., 2025) was introduced as a transformer-based model that is meta-learned by training on millions of synthetic datasets generated from specified priors.

### Novelty and Delineation from Prior Work

Our approach, POP, differs from prior work along sev-

eral key dimensions. Instead of meta-training on neural network losses (Shu et al., 2020; Xu et al., 2019; Metz et al., 2022), we train on a novel prior over convex and non-convex optimization problems, enabling meta-training over millions of synthetic functions at low computational cost. Rather than learning a global learning-rate schedule, POP predicts coordinate-wise learning rates. Using carefully designed input transformations such as boundary scaling, Z-transformation, and gradient scaling, POP exhibits strong generalization. Finally, coordinate-wise independence allows POP to scale naturally to high-dimensional settings via batching, while the transformer backbone efficiently processes long per-coordinate optimization histories.

Our work falls within meta-learning optimizers, where a model is trained to solve a distribution of optimization problems and generalize to unseen ones. We employ a transformer-based backbone that processes optimization trajectories and gradients to predict adaptive step sizes, effectively replacing classical solvers such as gradient descent. Operating at the algorithmic level, the learned model acts as a controller over the optimization process, modulating update directions and removing the need for hand-designed learning rate schedules.

## 8. Future Work

While our proposed method works well for optimization, its application to machine learning tasks remains an open direction that we leave to future work. A key challenge is designing synthetic priors that better reflect the structure of ML loss landscapes and generalize beyond function optimization. In addition, we plan to train the method on longer optimization trajectories and develop more compute-efficient policy architectures.

## 9. Conclusion

Optimization algorithms are central to minimizing functions, yet gradient-based methods that rely on first-order information often become trapped in local minima, limiting their ability to explore complex landscapes. We propose POP, a meta-learned optimizer that learns step size policies conditioned on the accumulated optimization history, enabling strategic escapes from local minima. POP is meta-trained on millions of synthetic optimization problems drawn from a novel Gaussian process prior, covering both convex and non-convex regimes. In a thorough evaluation, our model generalizes well and achieves strong performance on a well-established benchmark suite encompassing 47 diverse optimization functions. Overall, POP shows that state-conditioned learning rate policies, meta-trained on synthetic priors, enable robust and general-purpose optimization capabilities.

## Impact Statement

This paper presents work whose goal is to advance the field of Machine Learning. There are many potential societal consequences of our work, none which we feel must be specifically highlighted here.

## Acknowledgments

Josif Grabocka and Arlind Kadra acknowledge the funding support from the "Bayerisches Landesamt fur Steuer" for the Bavarian AI Taxation Laboratory.

Gresa Shala and Josif Grabocka acknowledge the funding by The Carl Zeiss Foundation through the research network "Responsive and Scalable Learning for Robots Assisting Humans" (ReScalE) of the University of Freiburg

Erind Bedalli and Josif Grabocka acknowledge the financial support from the Albanian-American Development Foundation through the READ program.

Moreover, we gratefully acknowledge the scientific support and HPC resources provided by the Erlangen National High Performance Computing Center (NHR@FAU) of the Friedrich-Alexander-Universität Erlangen-Nürnberg (FAU). NHR@FAU hardware is partially funded by the German Research Foundation (DFG) – 440719683.

## References

- Bergstra, J., Bardenet, R., Bengio, Y., and Kégl, B. Algorithms for hyper-parameter optimization. In *Advances in Neural Information Processing Systems*, volume 24, 2011.
- Cao, Y., Chen, T., Wang, Z., and Shen, Y. Learning to optimize in swarms. *Advances in neural information processing systems*, 32:15044–15054, 2019.
- Cauchy, A.-L. Méthode générale pour la résolution des systèmes d'équations simultanées. In *Comptes Rendus Hebdomadaires des Séances de l'Académie des Sciences*, 1847.
- Chen, T., Chen, X., Chen, W., Heaton, H., Liu, J., Wang, Z., and Yin, W. Learning to optimize: A primer and a benchmark. *J. Mach. Learn. Res.*, 23:189:1–189:59, 2021.
- Daoud, M. S., Shehab, M., Al-Mimi, H. M., Abualigah, L., Zitar, R. A., and Shambour, M. K. Y. Gradient-based optimizer (gbo): A review, theory, variants, and applications. *Archives of Computational Methods in Engineering*, 30 (4):2431–2449, December 2022. ISSN 1886-1784. doi: 10.1007/s11831-022-09872-y.
- Defazio, A., Yang, X., Khaled, A., Mishchenko, K., Mehta, H., and Cutkosky, A. The road less scheduled. *Advances in Neural Information Processing Systems*, 37: 9974–10007, 2024.
- Goldie, A. D., Lu, C., Jackson, M., Whiteson, S., and Foerster, J. Can learned optimization make reinforcement learning less difficult? *ArXiv*, abs/2407.07082, 2024. doi: 10.48550/arxiv.2407.07082.
- Gomes, H., Léger, B., and Gagn'e, C. Meta learning black-box population-based optimizers. *ArXiv*, abs/2103.03526, 2021.
- Gärtner, E., Metz, L., Andriluka, M., Freeman, C. D., and Sminchisescu, C. Transformer-based learned optimization, 2023.
- Hassan, E., Shams, M. Y., Hikal, N. A., and Elmoogy, S. The effect of choosing optimizer algorithms to improve computer vision tasks: a comparative study. *Multimedia Tools and Applications*, 82(11):16591–16633, September 2022. ISSN 1573-7721. doi: 10.1007/s11042-022-13820-0.
- Herbold, S. Autorank: A python package for automated ranking of classifiers. *Journal of Open Source Software*, 5(48):2173, 2020. doi: 10.21105/joss.02173.
- Holland, J. H. *Adaptation in Natural and Artificial Systems*. University of Michigan Press, Ann Arbor, 1992.
- Hollmann, N., Müller, S. G., Purucker, L., Krishnakumar, A., Körfer, M., Hoo, S. B., Schirrmeister, R., and Hutter, F. Accurate predictions on small data with a tabular foundation model. *Nature*, 637:319 – 326, 2025. doi: 10.1038/s41586-024-08328-6.
- Keskar, N. and Socher, R. Improving generalization performance by switching from adam to sgd. *ArXiv*, abs/1712.07628, 2017.
- Kingma, D. P. and Ba, J. Adam: A method for stochastic optimization. In Bengio, Y. and LeCun, Y. (eds.), *3rd International Conference on Learning Representations, ICLR 2015, San Diego, CA, USA, May 7-9, 2015, Conference Track Proceedings*, 2015.
- Kristiansen, G., Sandler, M., Zhmoginov, A., Miller, N., Goyal, A., Lee, J., and Vladymyrov, M. Narrowing the focus: Learned optimizers for pretrained models. *ArXiv*, abs/2408.09310, 2024. doi: 10.48550/arxiv.2408.09310.
- Lan, Q., Mahmood, R., Yan, S., and Xu, Z. Learning to optimize for reinforcement learning. *RLJ*, 2:481–497, 2023. doi: 10.48550/arxiv.2302.01470.

- Liao, L., Li, H., Shang, W., and Ma, L. An empirical study of the impact of hyperparameter tuning and model optimization on the performance properties of deep neural networks. *ACM Transactions on Software Engineering and Methodology (TOSEM)*, 31:1 – 40, 2022. doi: 10.1145/3506695.
- Liu, D. C. and Nocedal, J. On the limited memory bfgs method for large scale optimization. *Mathematical Programming*, 45(1):503–528, 1989.
- Liu, Y., Gao, Y., and Yin, W. An improved analysis of stochastic gradient descent with momentum. In *Proceedings of the 34th International Conference on Neural Information Processing Systems*, NIPS '20, Red Hook, NY, USA, 2020. Curran Associates Inc. ISBN 9781713829546.
- Ma, X., Zhong, Z., Li, Y., Li, D., and Qiao, Y. A novel reinforcement learning based heap-based optimizer. *Knowl. Based Syst.*, 296:111907, 2024. doi: 10.1016/j.knosys.2024.111907.
- Mary, A., Vincent, Member, I. P. J. S., and Member, I. A. A. B. S. Optimizing hyperparameters in meta-learning for enhanced image classification. *IEEE Access*, 13:130816–130831, 2025. doi: 10.1109/access.2025.3591142.
- Metz, L., Maheswaranathan, N., Freeman, C., Poole, B., and Sohl-Dickstein, J. N. Tasks, stability, architecture, and compute: Training more effective learned optimizers, and using them to train themselves. *ArXiv*, abs/2009.11243, 2020.
- Metz, L., Harrison, J., Freeman, C., Merchant, A., Beyer, L., Bradbury, J., Agrawal, N., Poole, B., Mordatch, I., Roberts, A., and Sohl-Dickstein, J. N. Velo: Training versatile learned optimizers by scaling up. *ArXiv*, abs/2211.09760, 2022. doi: 10.48550/arxiv.2211.09760.
- Moudgil, A., Knyazev, B., Lajoie, G., and Belilovsky, E. Celo: Training versatile learned optimizers on a compute diet. *Trans. Mach. Learn. Res.*, 2025, 2025.
- Müller, S., Hollmann, N., Arango, S. P., Grabocka, J., and Hutter, F. Transformers can do bayesian inference. In *International Conference on Learning Representations*, 2022.
- Newton, I. *Method of Fluxions and Infinite Series*. Henry Woodfall, 1736.
- Rahimi, A. and Recht, B. Random features for large-scale kernel machines. In *Neural Information Processing Systems*, 2007.
- Rasmussen, C. E. and Williams, C. K. I. *Gaussian Processes for Machine Learning*. The MIT Press, 2006.
- Robbins, H. and Monro, S. A stochastic approximation method. *Annals of Mathematical Statistics*, 22:400–407, 1951.
- Schlotthauer, J., Kroos, C., Hinze, C., Hangya, V., Hahn, L., and Küch, F. Pre-training llms on a budget: A comparison of three optimizers. *ArXiv*, abs/2507.08472, 2025. doi: 10.48550/arxiv.2507.08472.
- Schulman, J., Wolski, F., Dhariwal, P., Radford, A., and Klimov, O. Proximal policy optimization algorithms. *CoRR*, abs/1707.06347, 2017.
- Shu, J., Zhu, Y., Zhao, Q., Meng, D., and Xu, Z. Meta-lr-schedule-net: Learned lr schedules that scale and generalize, 07 2020.
- Storn, R. and Price, K. Differential evolution – a simple and efficient heuristic for global optimization over continuous spaces. *Journal of Global Optimization*, 11(4):341–359, 1997.
- Surjanovic, S. and Bingham, D. Virtual library of simulation experiments: Test functions and datasets. Retrieved December 14, 2025, from <http://www.sfu.ca/~ssurjan>.
- Tang, K. and Yao, X. Learn to optimize—a brief overview. *National Science Review*, 11(8), April 2024. ISSN 2053-714X. doi: 10.1093/nsr/nwae132.
- Tian, Y., Zhang, Y., and Zhang, H. Recent advances in stochastic gradient descent in deep learning. *Mathematics*, 2023. doi: 10.3390/math11030682.
- Vaswani, A., Shazeer, N., Parmar, N., Uszkoreit, J., Jones, L., Gomez, A. N., Kaiser, L. u., and Polosukhin, I. Attention is all you need. In Guyon, I., Luxburg, U. V., Bengio, S., Wallach, H., Fergus, R., Vishwanathan, S., and Garnett, R. (eds.), *Advances in Neural Information Processing Systems*, volume 30. Curran Associates, Inc., 2017.
- Vishnu, T., Malhotra, P., Narwariya, J., Vig, L., and Shroff, G. M. Meta-learning for black-box optimization. *Machine Learning and Knowledge Discovery in Databases*, 2020.
- Xu, Z., Dai, A. M., Kemp, J., and Metz, L. Learning an adaptive learning rate schedule. *arXiv preprint arXiv:1909.09712*, 2019.
- Yang, J., Chen, T., Zhu, M., He, F., Tao, D., Liang, Y., and Wang, Z. Learning to generalize provably in learning to optimize. *ArXiv*, abs/2302.11085, 2023. doi: 10.48550/arxiv.2302.11085.

## A. On the Universality of Gaussian Process Prior for Pretraining Learnable Optimizers

The statement that a Gaussian Process (GP) is a universal approximator is a consequence of the properties of its covariance function, or kernel. The universality is not inherent to all GPs but depends on the choice of a *universal kernel*. The proof relies on the connection between GPs and Reproducing Kernel Hilbert Spaces (RKHS). The approximation of the GP with Random Fourier Features introduces an additional approximation term absorbed into  $\epsilon$ .

**Theorem.** Let  $K \subset \mathbb{R}^d$  be a compact set. Let  $k : K \times K \rightarrow \mathbb{R}$  be a universal kernel. Let  $f \in C(K)$  be any continuous function on  $K$ . Then, for any  $\epsilon > 0$ , there exists a set of points  $X_n = \{x_1, \dots, x_n\} \subset K$  and corresponding values  $Y_n = \{f(x_1), \dots, f(x_n)\}$  such that the posterior mean  $\mu_n(x)$  of a Gaussian Process with prior mean  $m(x) = 0$  and kernel  $k(x, x')$  satisfies:

$$\sup_{x \in K} |f(x) - \mu_n(x)| < \epsilon.$$

### A.1. Preliminaries: Gaussian Processes and RKHS

A Gaussian Process  $GP(m(x), k(x, x'))$  is a stochastic process where any finite collection of random variables has a multivariate normal distribution. It is fully specified by its mean function  $m(x)$  and covariance function (kernel)  $k(x, x')$ . For simplicity, we assume a zero prior mean,  $m(x) = 0$ .

Given a set of  $n$  noiseless observations  $(X_n, Y_n) = \{(x_i, y_i)\}_{i=1}^n$  where  $y_i = f(x_i)$ , the posterior distribution of the GP at a new point  $x^*$  is also Gaussian. The posterior mean is given by:

$$\mu_n(x^*) = k(x^*, X_n) K_n^{-1} Y_n,$$

where  $k(x^*, X_n) = [k(x^*, x_1), \dots, k(x^*, x_n)]$  is a row vector and  $K_n$  is the  $n \times n$  Gram matrix with entries  $(K_n)_{ij} = k(x_i, x_j)$ .

Associated with every positive definite kernel  $k$  is a unique Reproducing Kernel Hilbert Space (RKHS), denoted  $\mathcal{H}_k$ . This is a Hilbert space of functions on  $K$  with two key properties:

1. For every  $x \in K$ , the function  $k_x(\cdot) := k(x, \cdot)$  is in  $\mathcal{H}_k$ .
2. (*Reproducing property*) For any  $g \in \mathcal{H}_k$  and  $x \in K$ , we have  $\langle g, k_x \rangle_{\mathcal{H}_k} = g(x)$ .

A crucial result from GP theory is that the posterior mean  $\mu_n(x)$  is the function in  $\mathcal{H}_k$  that minimizes the RKHS norm  $\|g\|_{\mathcal{H}_k}$  subject to the interpolation constraints  $g(x_i) = y_i$  for all  $i = 1, \dots, n$ .

### A.2. Universal Kernels

The approximation power of a GP is entirely determined by the richness of its RKHS. This leads to the definition of a universal kernel.

**Definition (Universal Kernel).** A continuous kernel  $k$  on a compact set  $K$  is called *universal* if its corresponding RKHS  $\mathcal{H}_k$  is dense in the space of continuous functions  $C(K)$  with respect to the uniform norm ( $L^\infty$ ).

This means that for any continuous function  $f \in C(K)$  and any  $\delta > 0$ , there exists a function  $g \in \mathcal{H}_k$  such that:

$$\sup_{x \in K} |f(x) - g(x)| < \delta.$$

Examples of universal kernels include:

- **Gaussian (RBF) Kernel:**

$$k(x, x') = \exp\left(-\frac{\|x - x'\|^2}{2\sigma^2}\right).$$

- **Matérn Kernels:**

$$k(x, x') = \frac{2^{1-\nu}}{\Gamma(\nu)} \left( \frac{\sqrt{2\nu} \|x - x'\|}{\ell} \right)^\nu K_\nu \left( \frac{\sqrt{2\nu} \|x - x'\|}{\ell} \right), \quad \nu > 0,$$

where  $K_\nu$  is the modified Bessel function of the second kind.

- **Laplacian Kernel:**

$$k(x, x') = \exp\left(-\frac{\|x - x'\|}{\sigma}\right).$$

The universality of these kernels is often established using characterizations like Bochner's theorem (a kernel is universal if its Fourier transform is positive on the entire frequency domain).

### A.3. Proof of the Theorem

Let  $k$  be a universal kernel on a compact set  $K$ , and let  $f \in C(K)$  be the target function. Let  $\epsilon > 0$  be the desired precision.

#### Step 1: Density of RKHS in $C(K)$

Since  $k$  is a universal kernel, its RKHS  $\mathcal{H}_k$  is dense in  $C(K)$ . Therefore, for our given  $\epsilon > 0$ , there exists a function  $g \in \mathcal{H}_k$  such that:

$$\sup_{x \in K} |f(x) - g(x)| < \frac{\epsilon}{2}.$$

#### Step 2: Convergence of the Interpolant

Now we need to show that we can choose data points  $X_n$  such that the GP posterior mean  $\mu_n(x)$  (which interpolates  $f$  on  $X_n$ ) becomes arbitrarily close to  $g(x)$ .

Let  $g$  be the function from Step 1. Since  $g \in \mathcal{H}_k$ , it has a finite RKHS norm,  $\|g\|_{\mathcal{H}_k} < \infty$ . Let us choose a sequence of points  $X_n = \{x_1, \dots, x_n\}$  that becomes dense in  $K$  as  $n \rightarrow \infty$ .

Let  $\mu_n^g$  be the GP posterior mean interpolating the values of  $g$  on  $X_n$ , i.e.,  $\mu_n^g(x_i) = g(x_i)$ . It is a standard result in the theory of RKHS (see Wendland, *Scattered Data Approximation*) that if  $X_n$  becomes dense in  $K$ , then the sequence of interpolants  $\mu_n^g$  converges uniformly to  $g$ :

$$\lim_{n \rightarrow \infty} \sup_{x \in K} |\mu_n^g(x) - g(x)| = 0.$$

Therefore, we can choose  $n$  large enough such that:

$$\sup_{x \in K} |\mu_n^g(x) - g(x)| < \frac{\epsilon}{2}.$$

#### Step 3: Combining the Approximations

Let  $\mu_n^f$  be the GP posterior mean interpolating the target function  $f$  on the same set of points  $X_n$ , i.e.,  $\mu_n^f(x_i) = f(x_i)$ .

The posterior mean is a linear operator on the data values. Let

$$L_n(Y)(x) = k(x, X_n)K_n^{-1}Y.$$

Then  $\mu_n^f = L_n(f(X_n))$  and  $\mu_n^g = L_n(g(X_n))$ .

We have:

$$\sup_{x \in K} |\mu_n^f(x) - \mu_n^g(x)| = \sup_{x \in K} |L_n(f(X_n) - g(X_n))(x)| \leq \|L_n\|_\infty \max_{i=1, \dots, n} |f(x_i) - g(x_i)|.$$

While  $\|L_n\|_\infty$  can grow with  $n$ , we can proceed using the triangle inequality:

$$\sup_{x \in K} |f(x) - \mu_n^f(x)| \leq \sup_{x \in K} |f(x) - g(x)| + \sup_{x \in K} |g(x) - \mu_n^g(x)| + \sup_{x \in K} |\mu_n^g(x) - \mu_n^f(x)|.$$

We have already bounded the first two terms. For the third term:

$$\mu_n^g(x) - \mu_n^f(x) = \sum_{i=1}^n c_i k(x, x_i),$$

where the coefficients satisfy

$$c = K_n^{-1} (g(X_n) - f(X_n)).$$

Hence,

$$\sup_{x \in K} |\mu_n^g(x) - \mu_n^f(x)| \leq C_n \max_i |g(x_i) - f(x_i)| < C_n \frac{\epsilon}{2},$$

where  $C_n$  depends on  $X_n$ .

A more elegant argument considers the projection of  $f$  onto the subspace spanned by  $\{k(x_i, \cdot)\}_{i=1}^n$ . The posterior mean  $\mu_n^f$  is precisely this projection. As  $n \rightarrow \infty$  and  $X_n$  becomes dense in  $K$ , the span of  $\{k(x_i, \cdot)\}_{i=1}^n$  becomes dense in  $\mathcal{H}_k$ .

Thus, the sequence  $\mu_n^f$  converges to the projection of  $f$  onto  $\mathcal{H}_k$ , denoted  $P_{\mathcal{H}_k} f$ . So, for large enough  $n$ :

$$\sup_{x \in K} |\mu_n^f(x) - P_{\mathcal{H}_k} f(x)| < \frac{\epsilon}{2}.$$

By the property of projections,  $P_{\mathcal{H}_k} f$  is the best approximation to  $f$  within  $\mathcal{H}_k$ . Since  $\mathcal{H}_k$  is dense in  $C(K)$ , we can find  $g \in \mathcal{H}_k$  such that  $\|f - g\|_\infty < \epsilon/2$ . This implies that  $\|f - P_{\mathcal{H}_k} f\|_\infty < \epsilon/2$ . Combining these gives:

$$\sup_{x \in K} |f(x) - \mu_n^f(x)| < \frac{\epsilon}{2} + \frac{\epsilon}{2} = \epsilon.$$

## Conclusion

The proof establishes that for any continuous function  $f$  and any precision  $\epsilon$ , one can find a finite set of sample points from  $f$  such that the posterior mean of a GP with a universal kernel approximates  $f$  to within  $\epsilon$  over the entire compact domain. The universality of the GP is therefore inherited directly from the denseness of its associated RKHS in the space of continuous functions. This is a powerful existence result, though it does not specify the number of points  $n$  required or the computational cost.

## B. Synthetic Prior

This appendix summarizes the parameterization of the synthetic prior used for meta-training (Table 4) and provides random visual examples of objective functions drawn from this prior (Figure 9).

Each function is generated by independently sampling all prior parameters and constructing the objective according to Section 3.

The resulting objectives vary naturally in scale, smoothness, curvature, and degree of non-convexity, reflecting the variability induced by the prior rather than any manual shaping of function landscapes.

### B.1. Parameter values of our proposed Prior

Table 4. Ranges and parameter values of the Prior.

Symbol	Distribution / Value
$D$	2
$M$	1000
$\beta^1$	$\mathcal{U}(10^{-8}, 10^{-2})$
$\beta^2$	$\mathcal{U}(-50, 50)$
$\alpha$	$\mathcal{U}(0.05, 0.4)$
$p_{\text{convex}}$	0.15
$\ell$	$\mathcal{U}(4, 8)$
$\sigma$	$\mathcal{U}(0.5, 3)$

### B.2. Visual Illustration of the Prior

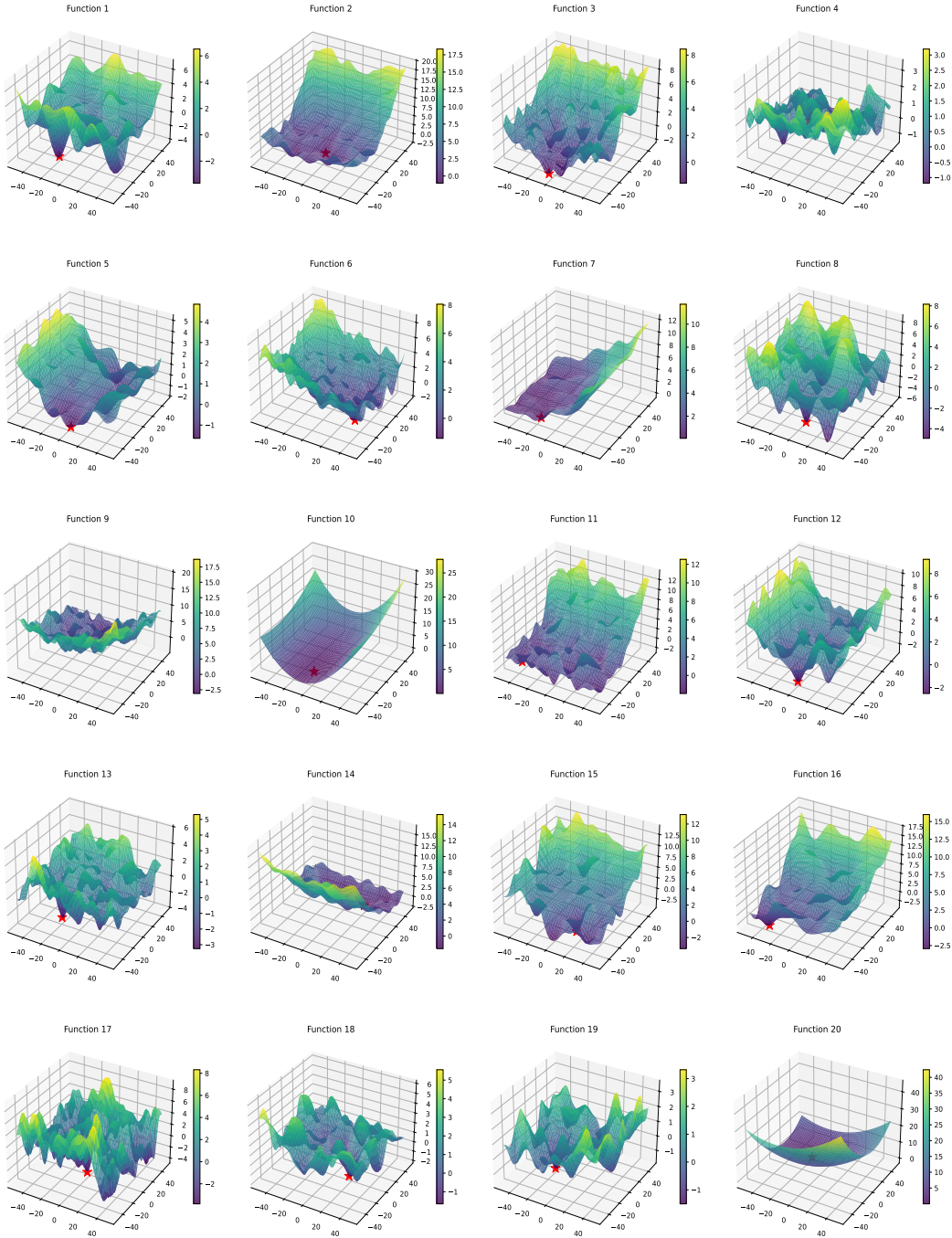


Figure 9. Exemplary functions sampled from the prior distribution (cf 3)

## C. Architecture and Training Details

This appendix reports the architectural and training hyperparameters used in all experiments. Unless stated otherwise, a single configuration is used across ablations and evaluations to isolate the effect of the proposed optimizer design from implementation-specific tuning. Table 5 summarizes the transformer-based architecture shared between actor and critic, while Table 6 details the PPO training setup and optimization hyperparameters. We set the boundary target scale as  $V_x = V_y = 3$ . Together, these settings fully specify the model and training procedure required to reproduce the reported results.

Table 5. Key architecture hyperparameters for the shared Transformer backbone and actor/critic heads.

Component	Value
<i>Shared backbone (Transformer)</i>	
Embedding dimension	64
# Transformer blocks	4
# Attention heads	4 ( $d_{\text{head}} = 16$ )
Dropout	0.05
Pooling	Last-token pooling
Shared output dim	32
<i>Actor / Critic heads</i>	
Actor head (MLP)	32 $\rightarrow$ 16 $\rightarrow$ 1
Critic head (MLP)	32 $\rightarrow$ 16 $\rightarrow$ 1

Table 6. PPO training hyperparameters and optimizer settings.

Component	Value
Actor lr	$1 \times 10^{-4}$
Critic lr	$1 \times 10^{-4}$
Optimizer	AdamWScheduleFree ( <a href="#">Defazio et al., 2024</a> )
Actor weight decay	$1 \times 10^{-4}$
Critic weight decay	$1 \times 10^{-4}$
Actor warmup	300
Critic warmup	10
PPO clip ratio	0.1
GAE $\gamma$	1.0
GAE $\lambda$	1.0
Epochs over collected trajectories	4
PPO Minibatch size	4096
Gradient clip norm	0.5
KL early stopping	0.01
Adaptive KL penalty	yes (initial coef 0.1, target KL 0.01)
Return normalization	Online Welford estimator

## D. Baseline Hyperparameter Optimization and Qualitative Analysis

This appendix contains additional experimental details that support the evaluation in Section 6. It is divided into two parts. First, we report the hyperparameter optimization (HPO) procedure used for baseline methods, including the learning-rate sweeps and selected configurations. These results ensure that all baselines are evaluated under competitive and well-tuned settings.

We sweep the initial learning rate for GD, Adam, and L-BFGS using a grid search over

$$\eta \in \{0.01, 0.02, 0.03, 0.05, 0.1, 0.2, 0.3, 0.5, 1.0, 2.0, 3.0, 5.0, 10.0, 20.0, 30.0, 50.0, 100.0\}.$$

All other hyperparameters are kept at their default values. For L-BFGS, this implies that the optimizer is allowed to perform more function evaluations per optimization iteration than the other baselines. Figure 10, Figure 11, and Figure 12 show the learning-rate sweeps for GD, Adam, and L-BFGS on the validation set, respectively.

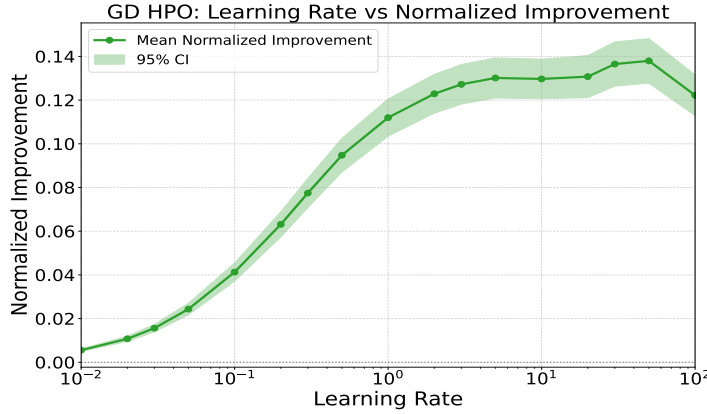


Figure 10. Learning rate sweep on the in-distribution validation set. Performance for GD peaks at a learning rate of 50.

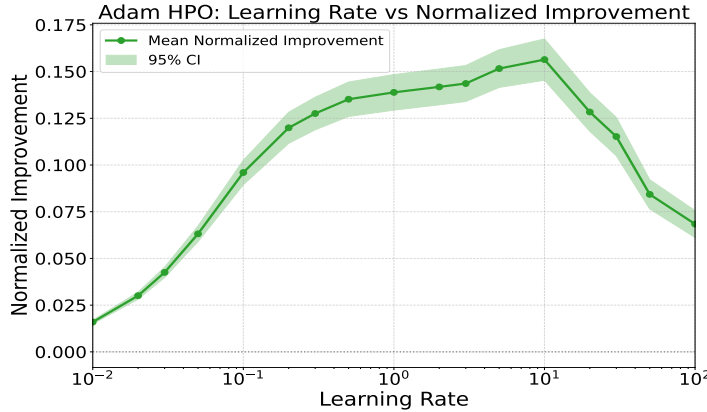


Figure 11. Learning rate sweep on the in-distribution validation set. Performance for Adam peaks at a learning rate of 10.

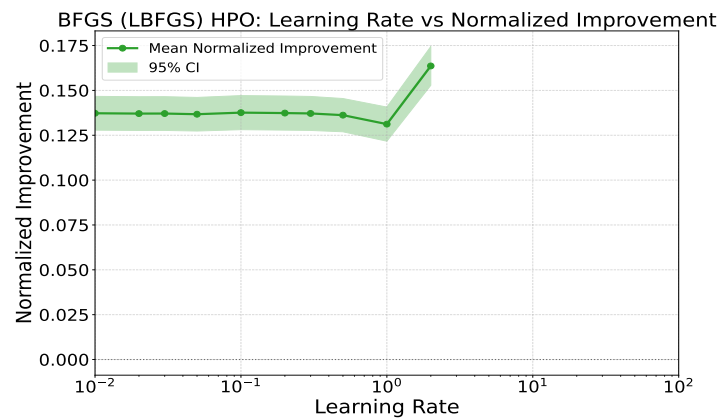


Figure 12. Learning rate sweep on the in-distribution validation set. Performance for L-BFGS peaks at a learning rate of 2. For learning rates  $> 2$ , the optimization problem fails and the normalized improvement is undefined (NaN)

### D.1. In-Distribution Performance

In the second part of this appendix, we provide qualitative visualizations of optimization trajectories produced by POP on functions sampled from the synthetic prior. These figures complement the quantitative results reported in Section 6 by illustrating typical optimization behaviors observed in practice.

They highlight how POP adapts its step sizes and exploration behavior in response to the local geometry of the objective function. In particular, the visualizations illustrate rapid convergence on convex objectives as well as adaptive exploration and escape from local minima in non-convex settings. Figure 13 and 14 show representative trajectories on convex and non-convex functions

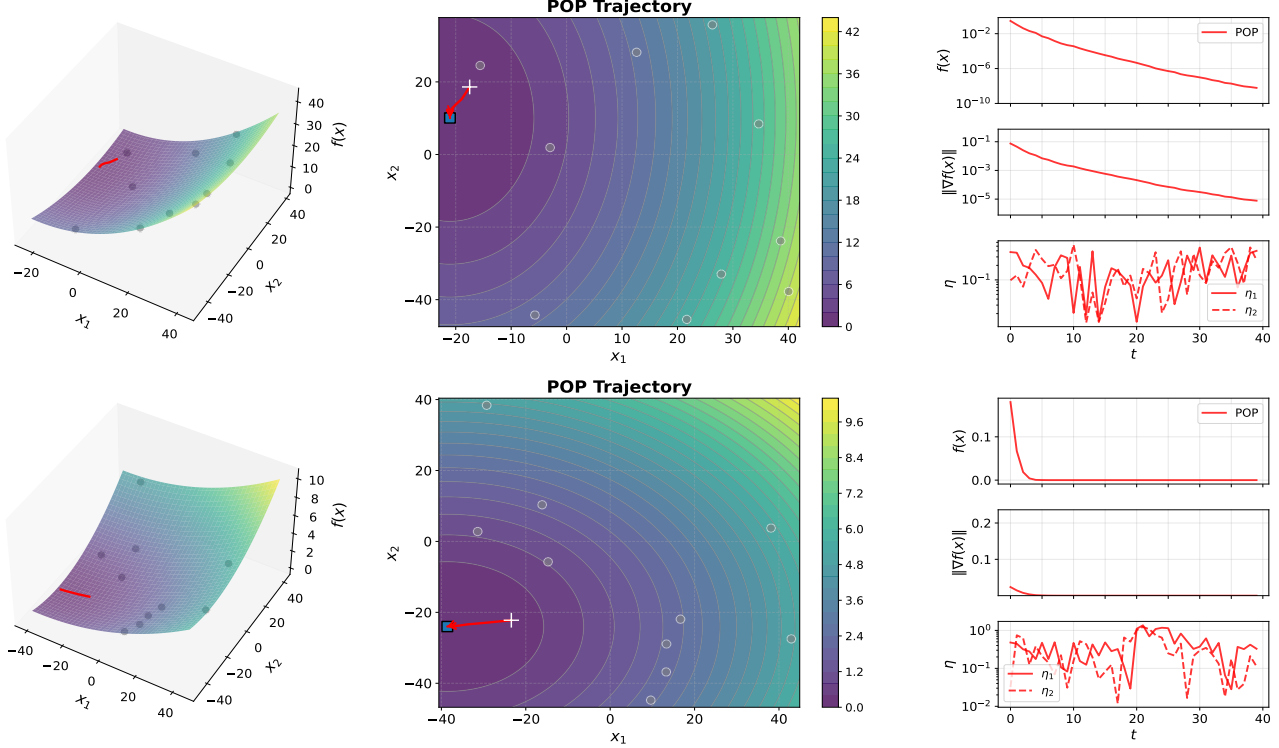


Figure 13. Trajectory of POP's on two convex functions. The algorithm progresses from the initial state (white cross) terminating at the final state (square).

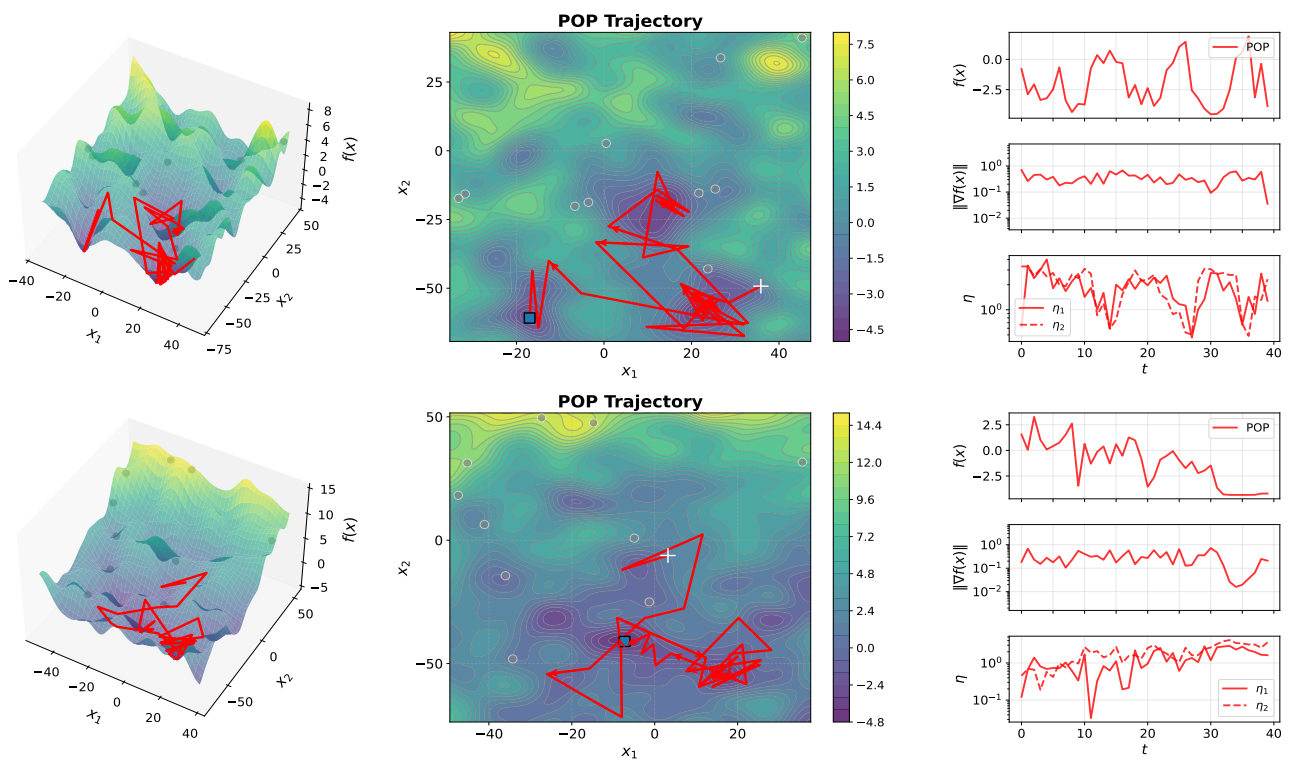


Figure 14. Trajectory of POP's on two non-convex functions. The algorithm progresses from the initial state (white cross) terminating at the final state (square).

## E. Virtual Library of Simulation Experiments benchmark

This appendix provides detailed results for the Virtual Library of Simulation Experiments (VLSE) benchmark used in Section 6. We report per-function normalized regret curves for all methods across the full optimization horizon. Each plot corresponds to a single benchmark function evaluated at its native dimensionality. All methods are run under identical evaluation budgets using the same performance metric, and no additional tuning or task-specific adjustments are performed.

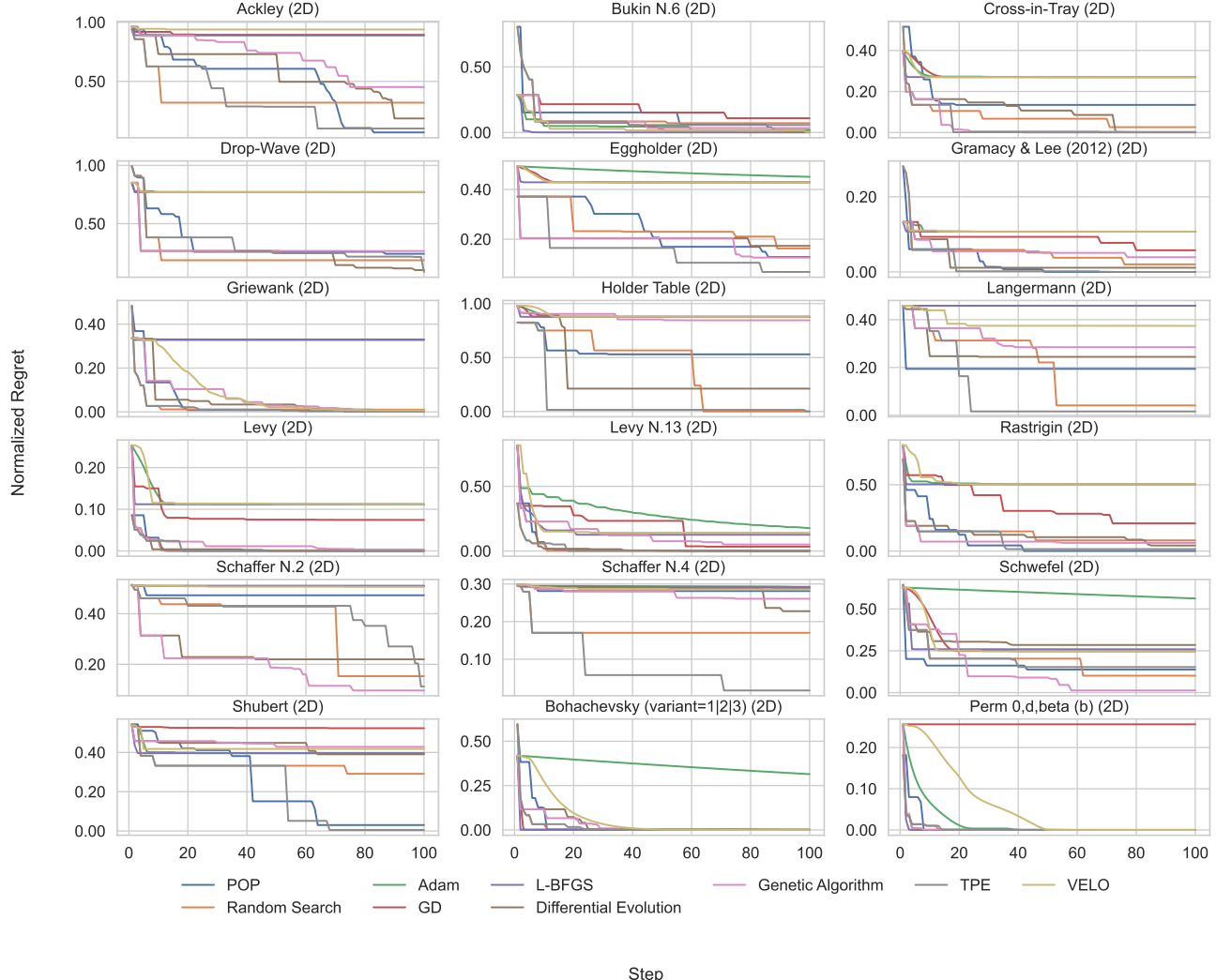


Figure 15. The normalized regret for all methods and functions 1 to 18. Solid lines represent the mean value.

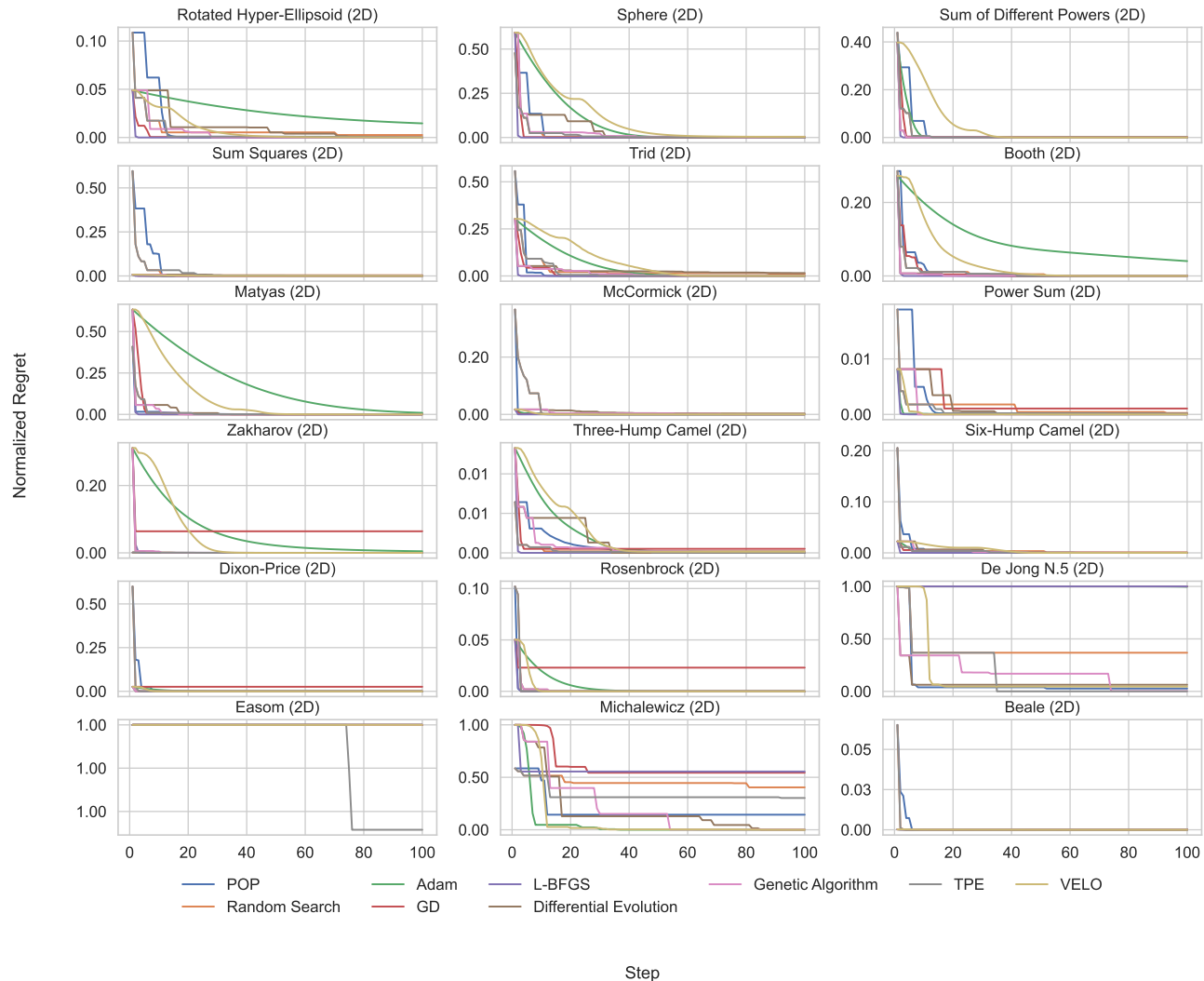


Figure 16. The normalized regret for all methods and functions 19 to 36. Solid lines represent the mean value.

## POP: Prior-fitted Optimizer Policies

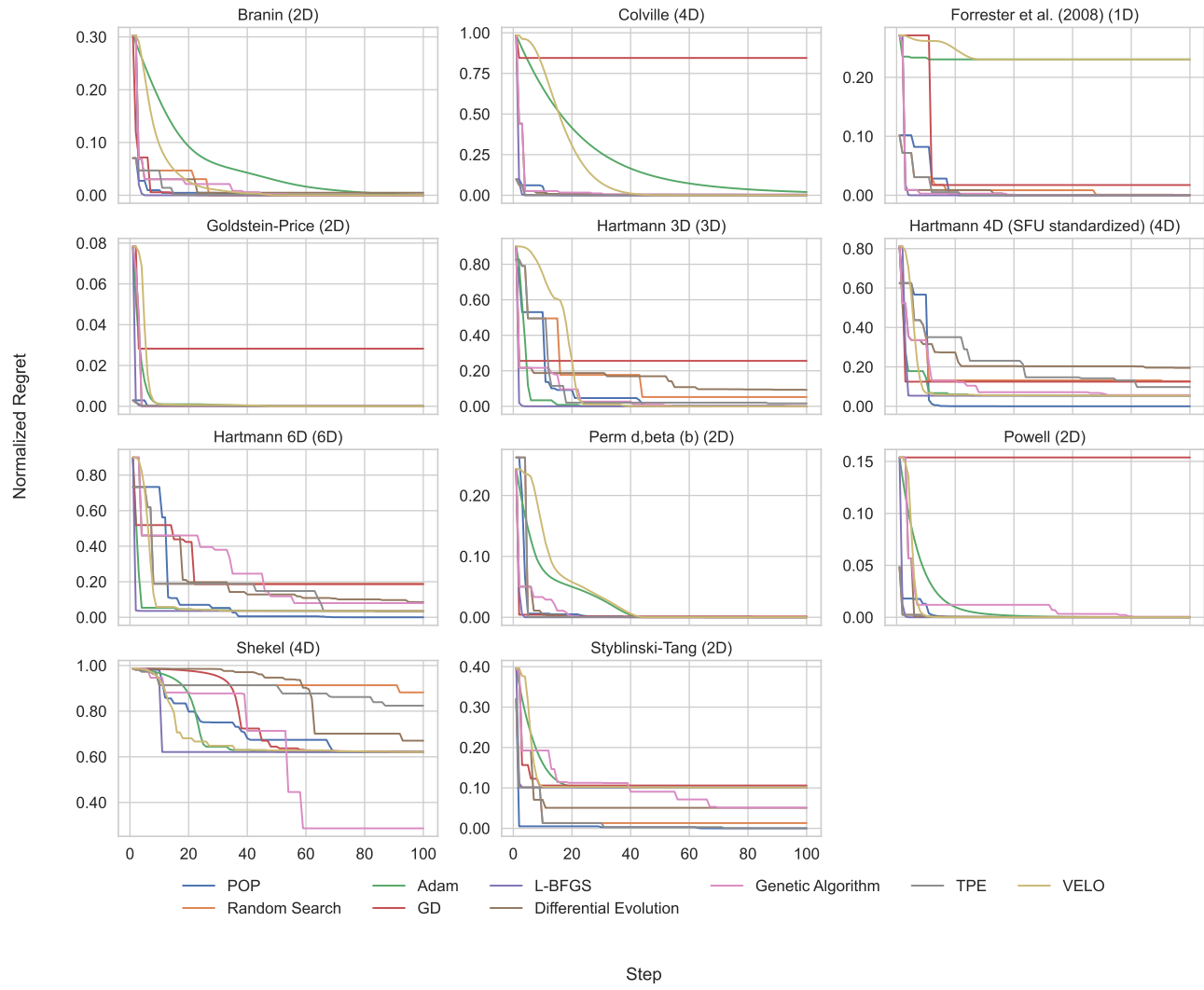


Figure 17. The normalized regret for all methods and functions 36 to 47. Solid lines represent the mean value.